Journal of Applied Biology & Biotechnology Vol. 15(1), pp. 181-195, January-February, 2027
Available online at http://www.jabonline.in
DOI: 10.7324/jabb.2026.319867

Green synthesis of silver, zinc oxide, and Ag–ZnO nanoparticles using *Syzygium cumini* leaf extract: Microwave-assisted synthesis, characterization, and biological activities

Shruti Jha, Priyanka Yadav, Dipti Gahlawat, Sandeep Singh*
Department of Biochemistry, Maharshi Dayanand University, Rohtak, India.

ARTICLE INFO

Article history:
Received on: 06/05/2026
Accepted on: 21/08/2026
Available Online: 25/11/2026

Key words:
Microwave synthesis, nanoparticles, characterization, antibacterial, antioxidant

ABSTRACT

This study reports the rapid microwave-assisted green synthesis of silver nanoparticles, zinc oxide (S-ZnO NPs), and silver-zinc oxide nanohybrid nanoparticles using *Syzygium cumini* (L.) leaf extract. The extract contained total phenolics (61.65 ± 2.24 mg gallic acid equivalents (GAE)/g extract) and total flavonoids (27.55 ± 0.81 mg quercetin equivalents/g extract). Nanoparticles were microwave-synthesized at 2450 MHz (800 W) and characterized by ultraviolet-visible spectroscopy (411, 361, and 345 nm), dynamic light scattering (125, 87, and 92 nm), zeta potential (-35, -23, and -14 mV), transmission electron microscopy (44.82 ± 10.94, 67.20 ± 12.19, and 41.96 ± 13.74 nm), scanning electron microscopy, Fourier transform infrared spectroscopy, and X-ray diffraction. Among the synthesized nanoparticles, S-Ag-ZnO NPs exhibited the highest antibacterial activity, with minimum inhibitory concentration / minimum bactericidal concentration values of 7.81/31.25 µg/ml against *Staphylococcus aureus* and 1.95/7.81 µg/ml against *Escherichia coli*, and inhibition zones of 11.35 ± 0.15 mm against *Bacillus subtilis* and 12.4 ± 0.4 mm against *Pseudomonas aeruginosa*. The *S. cumini* extract exhibited antibacterial activity only against *S. aureus* and *B. subtilis*. S-Ag-ZnO NPs exhibited IC_{50} values >12 µg/ml in the 2,2-diphenyl-1-picrylhydrazyl, 2,2-azino-bis-3-ethylbenzothiazoline-6-sulfonic acid, and superoxide scavenging assays and 614.62 ± 24.55 µg/ml in the p-NDA assay.

1. INTRODUCTION

Nanotechnology investigates materials as small as 100 nm that have high surface-to-volume ratios, hence increasing efficiency and adaptability. Metal oxide nanoparticles (NPs) are valued for their unique properties and wide applications, while medicinal plants provide a green, bioactive-rich source for their synthesis and biomedical use [1]. Phytochemicals including flavonoids, alkaloids, tannins, and phenolics play a crucial role in the medicinal properties of plants, contributing to their antibacterial, anti-inflammatory, and antioxidant effects [2]. Plant functional groups reduce metal ions to form NPs of varied sizes and shapes. Plant extract- or microbe-based green synthesis is safe for health and nature and is preferred over chemical synthesis in various biomedical applications [3]. Due to their facile synthesis, NPs are widely studied and applied in a range of fields, including electronics, sensing, imaging, coatings, catalysis, and medicine [4]. Ag-ZnO nanohybrid NPs consist of metallic Ag integrated with ZnO NPs, combining the complementary properties of both components. These nanohybrids have attracted considerable attention because of their enhanced functional performance compared with their individual constituents. AgNPs exhibit potent antibacterial activity through the release of Ag^+ ions, which disrupt bacterial cell membranes, proteins, and nucleic acids, whereas ZnO NPs exert antimicrobial effects primarily through the generation of reactive oxygen species (ROS) and the release of Zn^{2+} ions. Ag–ZnO nanohybrids have demonstrated promising antibacterial activity and are being investigated for potential applications against bacterial infections [5,6]. Monometallic AgNPs and ZnO NPs have also demonstrated significant potential for biosensing and diagnostic applications because of their unique optical, catalytic, and physicochemical properties [5]. Silver (Ag), copper (Cu), and zinc oxide (ZnO) are among the most widely investigated nanomaterials because of their unique physicochemical and biological properties. While Au/Ag NPs have well-established green synthesis approaches and biomedical applications, Ag-ZnO nanohybrid NPs have emerged as promising multifunctional nanomaterials with potential applications in environmental remediation, biomedicine, catalysis, and optics [6]. However, further investigation is still required into their synthesis methods and key features. *Syzygium cumini* L. (family Myrtaceae) is a traditional medicinal herb that originated in India and is extensively found in East Africa and Southeast Asia [7]. Among

*Corresponding Author
Sandeep Singh, Department of Biochemistry, Maharshi Dayanand University, Rohtak, India.
E-mail: ssingh.biochem @ mdurohtak.ac.in

© 2027 Shruti Jha *et al.* This is an open access article distributed under the terms of the Creative Commons Attribution License -NonCommercial-ShareAlike Unported License (http://creativecommons.org/licenses/by-nc-sa/3.0/).

the several pharmacological activities of *S. cumini*, an important medicinal plant, are antibacterial, anti-inflammatory, antioxidant, anticancer, antifungal, cardioprotective, and hepatoprotective qualities [8]. This is because it has wide therapeutic potential, being rich in phytochemicals. *Syzygium cumini* has various bioactive compounds such as acetyl-oleanolic acid, ellagic acid, triterpenoids, quercetin, iso-quercetin, myricetin, and kaempferol [9]. Catechin and ferulic acid are two examples of phenolic molecules that are primarily responsible for the antioxidant action of this substance [10]. In the present investigation, *S. cumini* leaf extract (S.E.) was used as a green reducing and stabilizing agent for the synthesis of nanomaterials. The extract contained a variety of bioactive phytochemicals with antioxidant properties that aid in the formation of monometallic *S. cumini*-derived silver NPs (S-AgNPs), *S. cumini*-derived ZnO NPs (S-ZnO NPs), and *S. cumini*-derived Ag-ZnO nanohybrid NPs (S-Ag-ZnO NPs).

In this context, the plant-mediated approach offers an alternative pathway for the synthesis of metal-based NPs with desired physicochemical and biological properties. The green synthesis of S-AgNPs, S-ZnO NPs, and S-Ag-ZnO nanohybrid NPs using S.E. is in accordance with the goals of the United Nations Sustainable Development Goals (UNSDGs), especially SDG 3 (Good Health and Well-being), SDG 9 (Industry, Innovation, and Infrastructure), and SDG 12 (Responsible Consumption and Production). The antibacterial and antioxidant activities of the synthesized NPs suggest their possible application in health care and environmental protection. Furthermore, the microwave-assisted synthesis approach has advantages such as shorter reaction time and may lead to more efficient use of resources compared with the conventional synthesis methods [11]. Thus, the present study highlights the scope of plant-mediated nanotechnology as a novel approach for the development of functional nanomaterials and the attainment of the larger goals of selected UNSDGs.

Microwave-assisted synthesis is widely used by many researchers for rapid and energy-efficient synthesis of metallic NPs. Microwave irradiation can speed up reaction rates by heating particular sites, which allows NPs with small particle sizes, narrow size distributions, and better stability to be formed [12]. There have been reports of green and microwave-assisted synthesis of Ag-ZnO NPs using a variety of plant extracts; however, to the best of our knowledge, the microwave-assisted synthesis of nanohybrid S-Ag-ZnO NPs using S.E. has not been investigated. Hence, the present work was undertaken in an effort to synthesize and compare the physicochemical properties, antibacterial activity, and antioxidant potential of the synthesized NPs.

The phytochemical-mediated synthesis provides a plant-based approach for the microwave-assisted green synthesis of S-AgNPs, S-ZnO NPs, and S-Ag-ZnO NPs using S.E. as both the reducing and stabilizing agent, without the addition of external chemical reducing agents. Under the experimental conditions employed in this study, the S-Ag-ZnO NPs exhibited comparatively higher antibacterial and antioxidant activities than the corresponding monometallic S-AgNPs and S-ZnO NPs. Collectively, these findings demonstrate the suitability of S.E. for the microwave-assisted green synthesis of these nanomaterials. The present study reports the biosynthesis, physicochemical characterization, antibacterial activity against the tested Gram-positive and Gram-negative bacterial strains, and antioxidant activity of the synthesized NPs. Nevertheless, quantitative sustainability metrics, direct comparison with conventionally synthesized NPs, and detailed mechanistic investigations were beyond the scope of the present study and remain subjects for future investigation.

2. MATERIALS AND METHODS

2.1. Materials and Reagents

The fresh *S. cumini* leaves were harvested from the Herbal Garden of Maharshi Dayanand University, Rohtak, India, in the month of September. The species was authenticated by Dr. Surender Singh Yadav of the Department of Botany, and a voucher specimen (MDU: 2021-105B) was archived in the university herbarium. Analytical-grade chemicals, including zinc acetate dihydrate ($Zn(CH_3COO)_2 \cdot 2H_2O$), silver nitrate ($AgNO_3$), 2,2-diphenyl-1-picrylhydrazyl (DPPH), 2,2-azino-bis-3-ethylbenzothiazoline-6-sulfonic acid (ABTS), sodium hydroxide (NaOH), and methanol, were used, with all solutions prepared in sterile double-distilled water (ddH_2O). Glassware was thoroughly cleaned and oven-dried before use.

2.2. Phytochemical extraction from *S. cumini*

Syzygium cumini leaves (10 g) were washed and air-dried, soaked in 100 ml of ddH_2O, and maintained at 60°C for 24 hours. In the present study, this extraction condition has been independently adopted and modified based on the experimental requirements of NPs synthesis. The resulting S.E. was filtered and stored at 4°C for further use as a reducing and stabilizing agent for the synthesis of NPs (Fig. 1a).

2.3. Estimation of total phenolics and flavonoids

The Folin-Ciocalteu (FC) method was employed to ascertain the total quantity of phenolics, with a few modifications [13]. The gallic acid calibration curve was employed to ascertain the polyphenolic concentration in the plant extract. In brief, 2.5 ml of 10% FC reagent and 2.5 ml of 7.5 % Na_2CO_3 solution were combined with 0.5 ml of gallic acid standard or plant aqueous extract. The absorbance

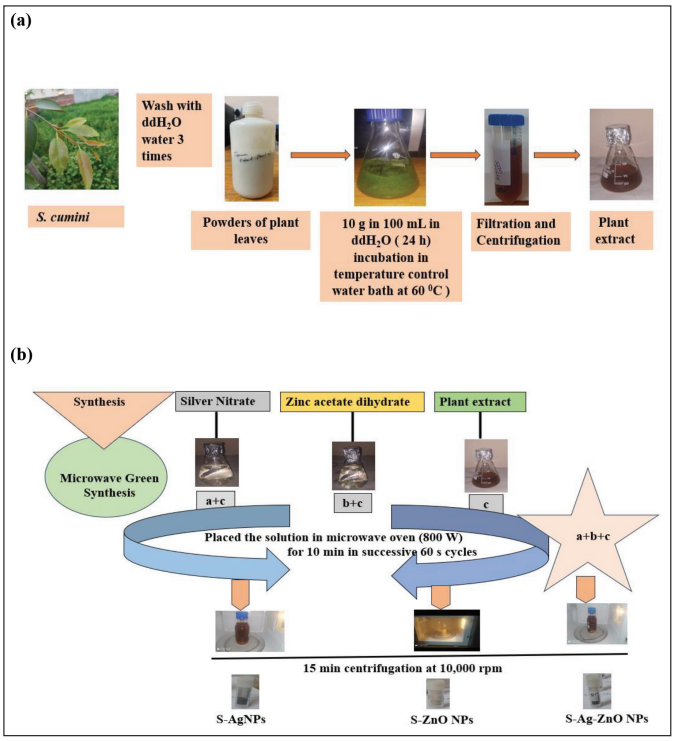

Figure 1. Diagrammatic representation of the synthesis process using (a) S.E. and (b) environmentally friendly S-AgNPs, S-ZnO NPs, and S-Ag-ZnO NPs synthesis.

was measured at 765 nm using an ultraviolet-visible (UV-vis) spectrophotometer after the reaction mixture was allowed to stand at ambient temperature for 1 hour.

The following formula was used to express TPC in mg GAE/g (mg gallic acid equivalents per gram of dry extract): TPC (mg GAE/g) = (X × V)/m

The calibration curve gives X (mg/ml) gallic acid concentration, V (ml) extract volume, and m (g) dry extract weight. The aluminum chloride colorimetric method evaluated total flavonoids with just minor adjustments [14]. A 5% sodium acetate solution, 1.5 ml of ethanolic aluminum chloride solution, and 0.5 ml of sample solution were combined, to sum it up. After 2.5 hours of incubation at room temperature, the absorbance was measured at 440 nm using a UV-vis spectrophotometer. Using quercetin as a reference, the total flavonoid concentration was determined as milligrams of quercetin equivalents per gram of dry extract [mg quercetin equivalents (QE)/g].

2.4. S-AgNPs, S-ZnO NPs, and S-Ag-ZnO NPs microwave synthesis

Microwave-assisted green synthesis method was employed to synthesize stable metallic NPs with a uniform size distribution. The synthesis of monometallic S-AgNPs was carried out in a domestic microwave oven (Sharp R-219T, 2450 MHz, 800 W) by adding 1 ml of S.E. to 100 ml of 1 mM $AgNO_3$ solution in a 250 ml borosilicate conical flask. The reaction mixture was irradiated with a microwave in 60-s cycles with cooling intervals between cycles, until the appearance of the characteristic dark brown color, which was always observed after a total irradiation time of about 10 minutes. A domestic microwave oven was used with a fixed power output and no real-time temperature monitoring or control was possible, so the reaction temperature was not experimentally measured. All syntheses were carried out with the same reaction conditions, such as precursor concentrations, reaction volume, reaction vessel, microwave power, and irradiation protocol, to ensure reproducibility. UV-visible spectroscopy further confirmed the formation of S-AgNPs. Microwave-assisted synthesis has also been reported to be an effective approach for the preparation of ZnO NPs [15]. The S-ZnO NPs were synthesized by mixing 100 ml of 0.01 M Zn $(CH_3COO)_2.2H_2O$ and 1 ml of leaf extract at pH 11 (adjusted with 1 M NaOH), resulting in a creamy white suspension [16]. The synthesis of S-Ag-ZnO NPs was carried out by mixing 40 ml of $AgNO_3$ solution (8 mM) and 40 ml of Zn $(CH_3 COO)_2 \cdot 2H_2O$ solution (0.4 M) with 10 ml of leaf extract in a 250 ml borosilicate conical flask and adjusting the pH to 11 with 1 M NaOH, yielding a final reaction volume of 100 ml. A greyish suspension was obtained by microwave irradiation under the same conditions. All NPs were collected by centrifugation at 10,000 rpm for 15 minutes, washed thrice with ddH_2O, and dried in a hot-air oven at 60°C for 2 hours. The obtained dry masses were approximately 25 mg of S-AgNPs, 100 mg of S-ZnO NPs, and 200 mg of S-Ag-ZnO NPs, respectively (Fig. 1b). The dried NPs were re-dispersed for biological evaluation, and different NPs concentrations were used for individual antibacterial and antioxidant assays as per the need and sensitivity of each experimental method.

The optimization of the synthesis conditions was done individually, as the formation of AgNP involves phytochemical reduction of Ag^+ and the formation of ZnO NP occurs by alkaline hydrolysis and crystallization of Zn^{2+}. Therefore, different precursor concentrations were tested, and a greater volume of standardized plant extract was used for synthesizing S-Ag-ZnO NPs to provide sufficient reducing and stabilizing phytochemicals. It should be noted that the synthesis conditions for S-AgNPs, S-ZnO NPs, and S-Ag-ZnO NPs were optimized individually according to their distinct formation mechanisms and therefore were not compositionally matched. Consequently, the present study does not include compositionally matched AgNP + ZnO physical mixture controls, metal-equivalent controls, or quantitative determination of the Ag:Zn elemental ratio. These aspects represent limitations of the current work and should be addressed in future studies to further distinguish compositional effects from nanohybrid-specific properties.

2.5. Instrumentation

The formation and surface plasmon resonance of NPs were monitored using UV-vis spectroscopy. Dynamic light scattering (DLS) and zeta potential, which links particle behavior to size, were used to analyze particle size and size distribution. DLS measurements were performed using a Malvern ZS-90 instrument. The dried NPs were dispersed in ddH_2O (0.5 mg/ml) and sonicated to give a homogeneous suspension prior to analysis. The measurements were performed at 25°C under the operating conditions given by the manufacturer. The DLS measurements consisted of 12 instrument runs for S-AgNPs and S-ZnO NPs and 14 instrument runs for S-Ag-ZnO NPs. The values represent the average from the instrument. Dried NPs were combined with potassium bromide to create 1% (w/w) pellets for Fourier transform infrared (FTIR) spectroscopy, and spectra were acquired in the 400–4,000 cm^{-1} range (Thermo Scientific IS 50). The crystalline nature was analyzed using X-ray diffraction (XRD) with Cu Kα radiation at 30 kV and 30 mA over a 2θ range of 5°–90°. Morphology and size structural features were further analyzed using scanning electron microscopy (SEM) (JEOL JSM 6610LV) and transmission electron microscopy (TEM) (TECNAI G20 HR-TEM, 200 kV). TEM was performed to examine the morphology and particle size of the synthesized NPs. Particle size analysis was carried out using ImageJ software by measuring 60 randomly selected NPs from three independent TEM micrographs (20 particles per micrograph) for each sample. The average particle size was expressed as mean ± standard deviation (SD), and the corresponding particle size ranges were determined from the measured particles.

2.6. Antimicrobial actions

2.6.1. Preparing strains of bacteria

Staphylococcus aureus MTCC-96 (*S. aureus*), *Bacillus subtilis* MTCC-2057 (*B. subtilis*), *Enterococcus faecium* ATCC-19434 (*E. faecium), Enterococcus faecalis* ATCC-19433 (*E. faecalis*), *Escherichia coli* ATCC-25922 (*E. coli*), *Klebsiella pneumoniae* MTCC-109 (*K. pneumoniae*), *Pseudomonas aeruginosa* MTCC-2453 (*P. aeruginosa*), and *Serratia marcescens* ATCC-14756 (*S. marcescens*) were obtained from the Department of Biochemistry of Maharshi Dayanand University Rohtak (Haryana, India). All of the bacterial strains were maintained for 24 h at 37 °C with stirring at 200 rpm in Mueller-Hinton broth (MHB).

2.6.2. Minimum inhibitory concentration testing, minimum bactericidal concentration testing, and disc diffusion method

An assessment was conducted to determine the minimum inhibitory concentration (MIC) and minimum bactericidal concentration (MBC) of NPs mediated by S.E. For MIC determination, the resazurin-based broth microdilution assay was performed according to established protocols. Briefly, a 96-well plate was treated with serially diluted NPs (500 to 0.97 µg/ml) and incubated for 18 hours at 37°C. Bacterial cultures were initiated by inoculating isolated colonies into MHB and incubating overnight at 37°C, followed by dilution in fresh medium to

achieve the mid-logarithmic growth phase (OD600 = 0.08–0.1). The suspension was adjusted to 0.5 McFarland turbidity and then diluted (1:100) to obtain a final inoculum concentration of 10^5–10^6 CFU/ml. These were growth control wells (medium + bacteria), sterility control wells (medium only), and wells for treatments containing NPs and bacteria. Resazurin dye was used as a viability indicator to determine the MIC. A blank control consisting of sterile MHB supplemented with resazurin dye was included in each assay and served as the reference for color interpretation. No unexpected color change attributable to NPs-induced optical or redox interference was observed during the resazurin-based MIC assay under the experimental conditions. The antibacterial activity determined by the resazurin assay was further corroborated using the disc diffusion assay, an interference-independent method.

A color change from blue to pink indicated metabolically active bacterial cells, whereas wells that remained blue indicated inhibition of bacterial growth. MBC values were established by subculturing 10 µl aliquots from wells displaying no apparent bacterial growth onto Mueller-Hinton agar plates and determining the lowest dose that generated no bacterial colonies during incubation, indicating bactericidal activity [17]. The antibacterial activity was assessed using the agar disc diffusion technique. Bacterial suspensions were evenly spread on agar plates and allowed to dry for 15 minutes. Sterile 5-mm discs loaded with 30 µl of NP samples or S.E. (200 µg/ml) were then placed on the inoculated plates. Antibacterial activity was assessed by the agar disc diffusion method using sterile Whatman filter paper discs (5-mm diameter). The use of 5-mm discs is comparable with previously described techniques for the evaluation of plant extracts and NP-based antibacterial agents. Accordingly, all inhibition zone diameters reported in this study are based on the 5-mm disc diameter [18]. Untreated discs served as negative controls with sterile ddH_2O, while ampicillin (10 µg/disc) was used as a positive control for most of the bacterial strains, and ciprofloxacin (5 µg/disc) was used for *K. pneumoniae, S. marcescens, and P. aeruginosa* bacterial strain. Following incubation at 37°C for 16–18 hours, zones of inhibition were measured [19]. All antibacterial assays were performed in triplicate ($n = 3$). The disc diffusion results are presented as mean ± SD, whereas the MIC and MBC values are reported as representative two-fold dilution endpoints obtained from three independent assay repetitions.

2.7. Antioxidant activities of S-AgNPs, S-ZnO NPs, and S-Ag-ZnO NPs

2.7.1. DPPH, ABTS, superoxide scavenging, and p-NDA Assays

The free radical scavenging ability of NPs was evaluated by the DPPH (2,2-diphenyl-1-picrylhydrazyl) test. Antioxidant activity was determined by the decolorization of a DPPH methanol solution from violet to yellow. Ascorbic acid (A.A), S.E., and NPs (2–12 µg/ml) were tested using 1 mM DPPH solution [20]. The antioxidant activity was measured by the scavenging of ABTS radicals generated from 7 mM ABTS (2,2′-azino-bis (3-ethylbenzothiazoline-6-sulfonic acid)) and 2.45 mM potassium persulfate using the ABTS assay. To generate ABTS radicals, the mixture of ABTS and potassium persulfate was kept in the dark for 12 hours. The ABTS radical solution obtained was then mixed with the tested samples and incubated for 30 minutes. The absorbance was then determined at 734 nm. The standard was A.A., and the control was the ABTS radical solution without NPs [21].

Superoxide radical-scavenging activity was determined using the riboflavin-light-nitro-blue tetrazolium (NBT) method [22]. In addition to 1 ml of the sample solution, the reaction volume (3 ml) included 50 mM phosphate buffer (pH 7.8), 13 mM methionine, 2 µM riboflavin, 100 µM EDTA, and 75 µM NBT. Blue formazan production was observed at 560 nm after 10 minutes of fluorescent light exposure. Increased superoxide anion scavenging activity, represented as percentage inhibition, was demonstrated by a reduction in absorbance. The reaction mixture for the hydroxyl radical scavenging assay using p-NDA (p-nitroso-dimethylaniline) contained ferric chloride (0.5 ml, 0.1 mM), EDTA (0.5 ml, 0.1 mM), A.A. (0.5 ml, 0.1 mM), hydrogen peroxide (0.5 ml, 2 mM), and p-NDA (0.5 ml, 0.01 mM) in 20 mM phosphate buffer (pH 7.4) with a final volume of 3 ml. To this, 0.5 ml of samples (NPs, S.E.) or standard (BHT) at concentrations ranging from 200 to 1,200 µg/ml was added. To produce a blank solution, 2.5 ml of phosphate buffer was combined with 0.5 ml of the sample. The absorbance of the blank solution was then measured at 440 nm [23].

$$\text{Percentage DPPH radical scavenging activity} = \frac{A_0 - A_1}{A_0} \times 100$$

Where A_0—Absorbance of the control

A_1—Absorbance of sample

IC_{50} values were calculated from the linear regression equation ($y = mx + c$) obtained by plotting percentage inhibition against concentration [24].

2.8. Statistics

All biological assays were performed in triplicate ($n = 3$). Continuous data are presented as mean ± SD, where applicable. One-way analysis of variance, followed by Tukey's post hoc test, was used to compare continuous variables, including inhibition zone diameters and antioxidant assay results. A p-value < 0.05 was considered statistically significant. MIC and MBC values were determined as discrete two-fold dilution endpoints from three independent assay repetitions and were not subjected to statistical analysis. Data were processed using Origin and statistically analyzed using IBM SPSS Statistics.

3. RESULT AND DISCUSSION

3.1. The sum of the phenolic and flavonoid contents

The total phenolic content of the S.E. was determined spectrophotometrically using the FC reagent. The gallic acid calibration equation was $Y = 0.0018x + 0.1028$ ($r^2 = 0.991$). The water extract of S.E. had a total phenolic content of 61.65 ± 2.24 mg GAE/g of plant extract. Using quercetin as a reference, the total flavonoid concentration in the S.E. was measured using a spectrophotometric technique. The quercetin calibration curve was used to derive the following linear equation: $Y = 0.0077x + 0.0109$ ($r^2 = 0.9867$). The following equation was used to determine the total flavonoid concentrations of S.E., which came out to 27.55 ± 0.81 mg QE/g of plant extract. The standard calibration curves are provided in (Fig. 2). S.E. has significant phenolic and flavonoid content, which helps to reduce and stabilize NPs during green synthesis.

Bioactive phytochemicals, especially phenolic and flavonoid compounds present in *S. cumini* leaves, may be involved in reduction and stabilization processes during NPs synthesis and thus may contribute to the antioxidant potential of the extract [25].

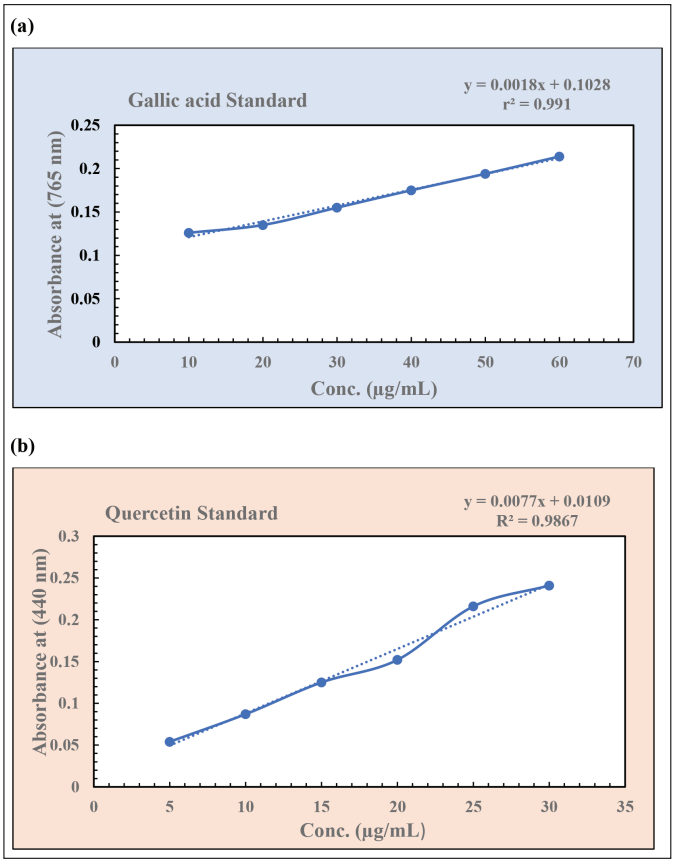

Figure 2. Standard calibration curve of (a) Gallic acid and (b) Quercetin, showing the linear relationship between absorbance and Standard concentration.

3.2. UV-vis analysis of S-AgNPs, S-ZnO NPs, and S-Ag-ZnO NPs

The UV-vis spectra confirmed the successful synthesis of NPs using S.E., as depicted in (Fig. 3). The plant extract exhibited no distinct absorption peak, whereas S-AgNPs showed a characteristic localized surface plasmon resonance (LSPR) peak at 411 nm, confirming the formation of S-AgNPs, and S-ZnO NPs displayed a band-edge absorption at 361 nm, characteristic of S-ZnO NPs. In contrast, the S-Ag-ZnO NPs had a single absorption band at 345 nm rather than a simple combination of the separate Ag and ZnO absorption properties. The observed blue shift relative to the monometallic NPs indicates a reduction in particle size and may reflect changes in the optical properties associated with the combined presence of Ag and ZnO in the nanohybrid NPs. Such changes in the LSPR characteristics are commonly associated with variations in particle size, composition, and the local physicochemical environment of the NPs. Thus, UV-vis spectroscopic analysis confirmed the formation of the NPs and gave information about the optical properties and particle size. In a previous study of ZnO/Ag nanohybrids, a typical plasmon absorption band of AgNPs around 410 nm was observed, and the optical absorption characteristics were altered by the incorporation of Ag with ZnO [26]. The spectral shifts observed for the green-synthesized S-Ag-ZnO NPs are comparable with those reported previously and may reflect changes in the optical properties associated with the combined presence of Ag and ZnO. However, the specific interactions between these components were not directly investigated in the present study.

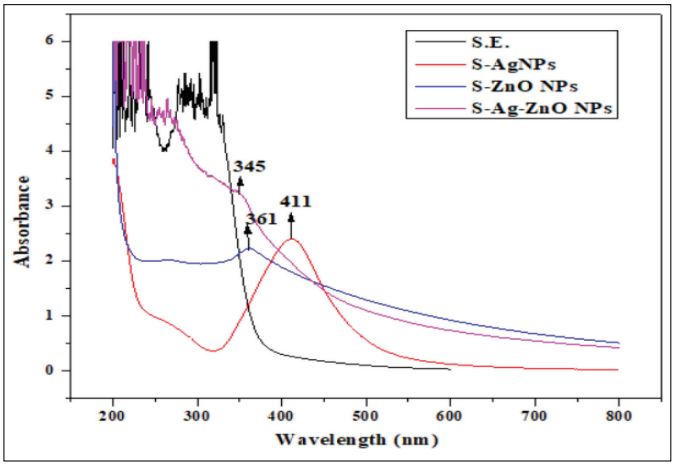

Figure 3. UV-vis spectra of S.E., S-AgNPs, S-ZnO NPs, and S-Ag-ZnO NPs.

3.3. Evaluation of S-AgNPs, S-ZnO NPs, and S-Ag-ZnO NPs by Zeta potential and DLS measurements

The zeta potential analysis showed that all synthesized NPs possessed negatively charged surfaces. S-AgNPs, S-ZnO NPs, and S-Ag-ZnO NPs exhibited zeta potential values of −35 mV, −23 mV, and −14 mV, respectively, as shown in (Fig. 4a, c, and e). The S-AgNPs exhibited the highest negative zeta potential, suggesting greater electrostatic stabilization of the freshly prepared dispersion. NPs with zeta potential values greater than +30 mV or lower than −30 mV are generally considered to possess good electrostatic stability due to increased interparticle repulsion [27]. In contrast, the reduced absolute zeta potential values observed for S-ZnO NPs and S-Ag-ZnO NPs indicate comparatively reduced electrostatic stabilization. The negative surface charge of all NPs formulations is in agreement with the adsorption of phytochemicals from the S.E., which probably served as reducing and surface-capping agents during synthesis [28]. The hydrodynamic particle sizes of the synthesized NPs were determined by DLS, which measures particle size in suspension based on Brownian motion and light scattering (Fig. 4b, d, and f). The average hydrodynamic diameters of S-AgNPs, S-ZnO NPs, and S-Ag-ZnO NPs were 125 nm, 87 nm, and 92 nm, respectively. These values were larger than those obtained by TEM because DLS measures the hydrodynamic diameter, including the hydration layer, adsorbed phytochemicals, and particle agglomeration, whereas TEM measures the dry particle core [29]. The polydispersity index (PDI) values for S-AgNPs, S-ZnO NPs, and S-Ag-ZnO NPs were found to be 0.508, 1.000, and 0.682, respectively. These values show different levels of heterogeneity in particle size among the synthesized NPs. The PDI of S-AgNPs is a medium-wide distribution of particle size. The S-Ag-ZnO NPs showed a wider polydisperse distribution. The PDI value of 1.000 for S-ZnO NPs means a very heterogeneous particle population, which may be due to aggregation and/or the existence of several particle size populations. Such broad hydrodynamic size distributions are often reported for plant-mediated NPs, as DLS is sensitive to particle agglomeration and the presence of surface-bound phytochemicals [30]. Thus, the DLS and zeta potential analyses provide information on the hydrodynamic behavior and surface charge of the freshly prepared NP dispersions under the experimental conditions employed. However, these measurements should not be regarded as conclusive evidence of long-term colloidal stability, which would require additional time-dependent stability studies.

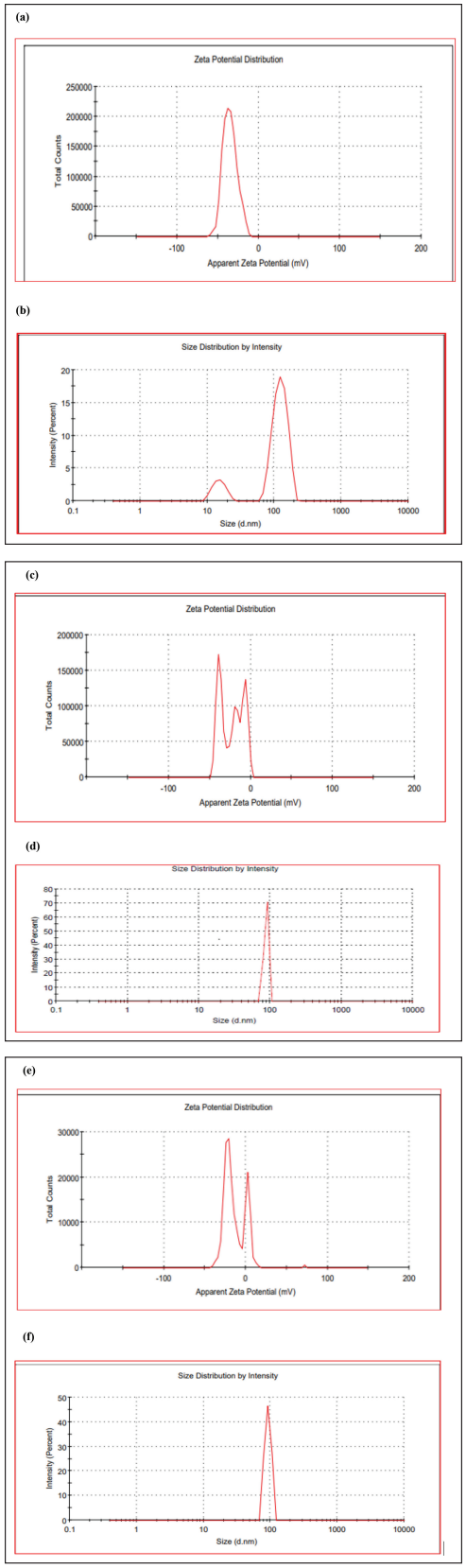

Figure 4. Size distribution of NPs obtained from zeta potential and DLS: (a) S-AgNPs (-35 mV), (b) S-AgNPs (125 nm), (c) S-ZnO NPs (-23 mV), (d) S-ZnO NPs (87 nm), (e) S-Ag-ZnO NPs (-14 mV), and (f) S-Ag-ZnO NPs (92 nm).

3.4. Characterization by FTIR

The FTIR spectrum of the S.E. extract showed characteristic peaks at 3481, 1578, 2058, 1218, and 1043 cm^{-1}. The O–H stretching vibrations of phenolic and alcoholic groups are represented by the wide band at 3481 cm^{-1} [32]. The absorption band at 1578 cm^{-1} is thought to be caused by N–H bending vibrations or aromatic C=C stretching, whereas the peak at 2058 cm^{-1} could be related to CO_2 or C–C stretching. The peaks observed at 1218 and 1043 cm^{-1} are assigned to C–O and C–N stretching vibrations, respectively, indicating the presence of phenols, ethers, alcohols, polysaccharides, and amine groups, as shown in (Fig. 5a) [31]. For S-AgNPs, the peaks at 1640, 1380, and 980 cm^{-1} are caused by C=O or aromatic C=C vibrations, C–H bending or C–N stretching, and C–O stretching, respectively, as shown in (Fig. 5b). These functional groups, when compared to extracts, indicate the active role of proteins and polyphenols in the reduction and stabilization of NPs [33]. S-ZnO NPs showed peaks at 3381, 1612, 1483, 1403, and 900 cm^{-1}, as shown in (Fig. 5c). These peaks were attributed to O–H stretching, C=O (amide)/C=C vibrations, C–H bending, C–N stretching, and Zn–O stretching, respectively. The broad band at 3381 cm^{-1} was due to the stretching vibrations of O–H, which confirms the presence of phenolic compounds in the synthesis of NPs. The band at 1612 cm^{-1} was ascribed to aromatic C=C vibrations or C=O stretch of amide groups, indicating the incorporation of proteins and phytochemicals in the capping. The peaks at 1483 and 1403 cm^{-1} are the C–H bending and C–N stretching vibrations, respectively, which show the presence of organic residues like proteins and amines that favor the stabilization of NPs. A peak at 900 cm^{-1} is ascribed to the Zn-O stretching vibration, confirming the effective production of S-ZnO NPs [34]. The characteristic absorption bands of the S-Ag-ZnO NPs were observed at 3508, 1629, 1504, 1067, and 905 cm^{-1}, respectively, indicating the presence of O–H stretching, amide or aromatic C=C vibrations, aromatic C=C or N–H bending, C–O/C–N stretching, and the formation of a Zn-O bond (Fig. 5d) [35]. The detection of O–H, C–O, and C–N functional groups confirms the existence of phenolic substances, flavonoids, tannins, proteins, and polysaccharides in the extract, which serve as reducing and stabilizing agents during FTIR analysis. The changes in O–H and amide-related peaks after NPs formation suggest that these biomolecules are actively involved in the reduction of metal ions and capping of NPs [36]. The presence of the Zn-O stretching vibration in the S-ZnO NPs and its retention in the S-Ag-ZnO NPs confirm the presence of ZnO in the synthesized NPs. Overall, the FTIR analysis indicates that plant-derived phytochemicals likely contributed to the reduction and stabilization of the monometallic and nanohybrid NPs by acting as reducing and capping agents [37].

3.5. XRD of S-AgNPs, S-ZnO NPs, and S-Ag-ZnO NPs

XRD was used for the characterization of the crystalline structure of the synthesized S-AgNPs, S-ZnO NPs, and S-Ag-ZnO NPs. The diffraction patterns were in agreement with the standard JCPDS files for face-centered cubic (fcc) Ag (JCPDS No. 04-0783) and hexagonal wurtzite ZnO (JCPDS No. 79-2205), suggesting the crystalline nature of the synthesized NPs. As shown in (Fig. 6a), S-AgNPs had diffraction peaks at 38.20°, 44.14°, 64.50°, and 77.38° corresponding to the (111), (200), (220), and (311) crystallographic planes of metallic Ag, respectively [38]. Similarly, the diffraction peaks of S-ZnO NPs obtained at 31.76°, 34.42°, 36.24°, 47.56°, 56.58°, 62.82°, and 67.92° were indexed to the (100), (002), (101), (102), (110), (103), and (112) planes of hexagonal ZnO, respectively (Fig. 6b). The XRD pattern of S-Ag-ZnO NPs (Fig. 6c) showed characteristic diffraction peaks for crystalline Ag and ZnO at 31.76°, 34.44°, 36.28°, 38.14°, 44.26°, 47.48°, 56.66°, 62.82°, 67.92°,

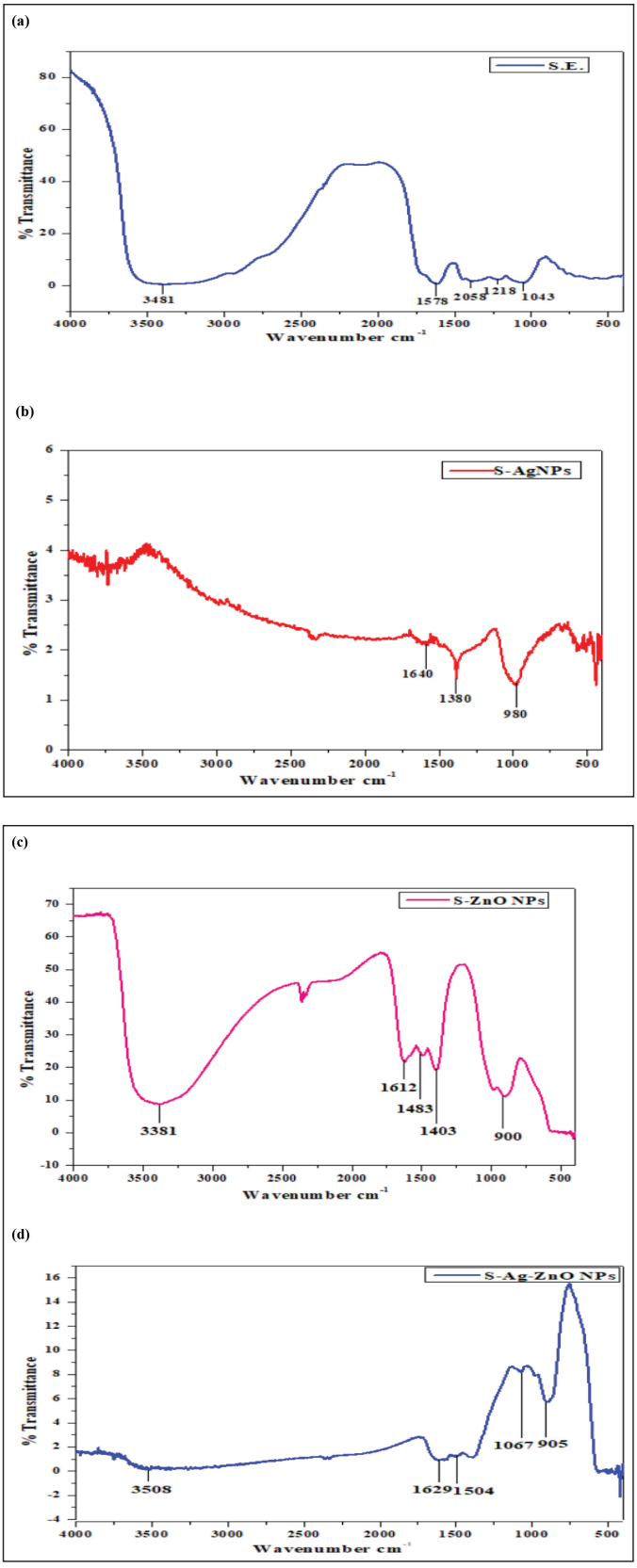

Figure 5. FTIR spectra of (a) S.E., (b) S-AgNPs, (c) S-ZnO NPs, and (d) S-Ag-ZnO NPs.

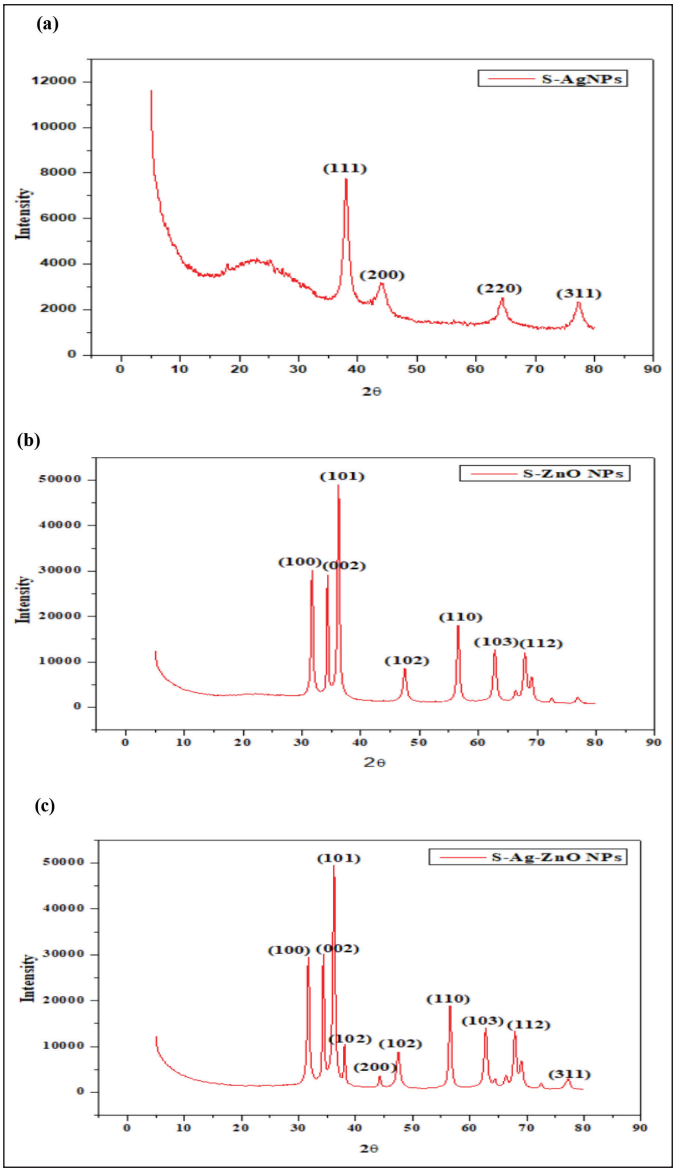

Figure 6. XRD patterns of NPs: (a) S-AgNPs, (b) S-ZnO NPs, and (c) S-Ag-ZnO NPs.

and 77.36°, confirming the presence of both crystalline phases in the synthesized sample [39]. However, XRD results alone do not provide evidence for nanoscale integration, Ag incorporation into or onto ZnO, or the formation of well-defined S-Ag-ZnO NPs. The crystallite size was calculated based on the Scherrer equation ($D = K\lambda/\beta\cos\theta$), where K is the shape factor (0.9), λ is the wavelength of Cu Kα radiation (1.5406 Å), β is the full width at half maximum, and θ is the Bragg angle [40]. Lattice strain ($\varepsilon=\beta/4\tan\theta$) and dislocation density ($\delta=1/D^2$) were also calculated. Average crystallite sizes of S-AgNPs, S-ZnO NPs, and S-Ag-ZnO NPs were 7.11, 18.04, and 15.83 nm, respectively. The respective values of lattice strain and dislocation densities were 0.01498, 0.00702, 0.00799, and 1.98×10^{-2}, 3.07×10^{-3}, and 3.99×10^{-3} nm^{-2}. XRD analysis confirmed good crystallinity and nanoscale crystallite sizes of the synthesized NPs and confirmed the coexistence of crystalline Ag and ZnO phases in the S-Ag-ZnO NPs.

3.6. Microscopic Examinations (SEM and TEM)

The synthesized NPs were further characterized by SEM to study the surface morphology and structural features and TEM to study

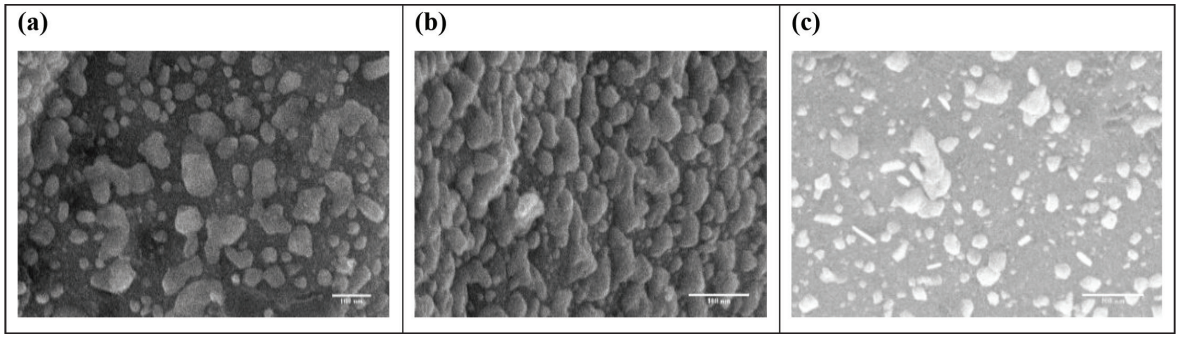

Figure 7. SEM images of (a) S-AgNPs, (b) S-ZnO NPs, and (c) S-Ag-ZnO NPs.

the particle morphology and size distribution (Figs. 7 and 8). SEM analysis showed that S-AgNPs (Fig. 7a) were mainly spherical with some agglomeration, while S-ZnO NPs (Fig. 7b) were heterogeneous aggregated nanostructures containing primary NPs of different shapes. However, S-Ag-ZnO NPs (Fig. 7c) showed NPs which are fairly well dispersed, with faceted and anisotropic morphologies and relatively less agglomeration. The mean particle sizes, calculated by measuring 60 individual particles from three representative TEM images using ImageJ software, were 44.82 ± 10.94 nm, 67.20 ± 12.19 nm, and 41.96 ± 13.74 nm for S-AgNPs, S-ZnO NPs, and the S-Ag-ZnO NPs, respectively (histograms of the particle size distribution are shown in (Fig. 8a–c). The average particle size of the S-Ag-ZnO NPs was relatively smaller, which may be due to the simultaneous synthesis conditions affecting nucleation and growth of the particles. However, the TEM observations are limited to particle morphology and size only and do not themselves provide evidence for Ag incorporation in ZnO or for the formation of a well-defined Ag-ZnO heterostructure. The observed morphological differences may be related to differences in the precursor chemistry and phytochemical-mediated nucleation and crystal growth. The phytochemicals present in the S.E. may have acted as reducing and capping agents and possibly influenced the growth of the particles by preferential interaction with the different crystal facets.

Hence, S-AgNPs mainly showed spherical morphological features, whereas S-ZnO NPs exhibited heterogeneous and aggregated structures, which reflects the differences in physicochemical properties and growth characteristics of the respective NPs systems [41]. The relatively smaller particle size and lower agglomeration of S-Ag-ZnO NPs may be attributed to the capping and stabilizing effects of phytochemicals contained in the S.E., which may influence the NPs' nucleation, growth, and aggregation during synthesis. In summary, the UV-Vis, FTIR, DLS, zeta potential, XRD, TEM and SEM studies gave complementary information on the optical properties, surface functional groups, hydrodynamic behavior, crystalline phases, particle morphology and particle size of the synthesized NPs. However, while these techniques confirmed crystalline Ag and ZnO phases and nanoscale morphology, further characterization techniques such as STEM–EDS elemental mapping, HRTEM/SAED, or XPS are required to verify the nanoscale architecture, elemental distribution, and interfacial interactions between Ag and ZnO components [42].

3.7. Antibacterial activities

The antibacterial activities of synthesized S-AgNPs, S-ZnO NPs, and S-Ag-ZnO NPs were quantitatively evaluated using MIC and MBC against Gram-positive and Gram-negative bacterial strains. Among the synthesized NPs, the S-Ag-ZnO NPs displayed the minimum MIC and MBC values against all tested bacterial strains, suggesting that lower concentrations are needed to inhibit bacterial growth and to achieve bactericidal activity under the experimental conditions. The MIC/MBC of S-Ag-ZnO NPs were 7.81/31.25, 3.9/15.625, 7.81/31.25, and 15.625/62.5 µg/ml against Gram-positive bacteria, *S. aureus*, *E. faecium*, *E. faecalis,* and *B. subtilis*, respectively. These values were lower than those observed for the corresponding S-AgNPs and S-ZnO NPs but higher than those of the reference antibiotic ampicillin. The S.E. showed no measurable antibacterial activity against most of the bacterial strains tested except *S. aureus* and *B. subtilis*. S-AgNPs exhibited moderate antibacterial activity, and S-ZnO NPs showed the highest MIC and MBC values among all synthesized NPs. A similar tendency was found for the Gram-negative bacteria. The lowest observed MIC/MBC values were obtained with S-Ag-ZnO NPs against *E. coli* (1.95/7.81 µg/ml) and *P. aeruginosa* (7.81/31.25 µg/ml), respectively. S-ZnO NPs were found to have comparatively higher MIC and MBC values than the other NPs formulations. The antibacterial activity of ampicillin and ciprofloxacin was higher than that of all the synthesized NPs, while the S-Ag-ZnO NPs exhibited the highest antibacterial activity among the NPs formulations under the experimental conditions (Table 1). Dedicated NPs-only interference controls were not included in the present study, but no evidence of NPs-induced color interference was seen during the resazurin-based MIC assay under the experimental conditions. Moreover, the consistency between the resazurin-based MIC assay and the interference-free disc diffusion assay supports the notion that NPs interference was unlikely to have contributed significantly to the antibacterial activity observed. However, inclusion of NPs-only interference controls would be beneficial for future investigations. The synthesized NPs were further evaluated for their antibacterial activity using a disc diffusion assay against Gram-positive and Gram-negative bacterial strains at a concentration of 200 µg/ml. The results were in agreement with those obtained from MIC and MBC assays. All synthesized NPs exhibited detectable antibacterial activity against both Gram-positive and Gram-negative bacteria, although differences in inhibition zones were observed among the tested samples. The synthesized S-Ag-ZnO NPs exhibited relatively larger inhibition zones against all the bacterial strains among the formulated NPs. The inhibition zones for Gram-positive bacteria ranged from 9.8 ± 0.2 mm (*S. aureus*) to 11.35 ± 0.15 mm (*B. subtilis*). The largest inhibition zones were observed against *P. aeruginosa* and *S. marcescens* (12.4 ± 0.4 mm and 12.25 ± 0.25 mm, respectively), indicating antibacterial activity against both groups of bacteria. S-AgNPs showed moderate antibacterial activity with inhibition zones ranging from 7.9 ± 0.1 mm to 11.15 ± 0.15 mm, while S-ZnO NPs generally showed smaller inhibition zones ranging from 5.85 ± 0.15 mm to 8.25 ± 0.25 mm. The S.E. extract showed low antibacterial activity, with an inhibition zone observed only against *S. aureus* (5.5 ± 0.7 mm) and no detectable inhibition zone against the remaining bacterial strains. Generally, all the NPs formulations showed lower antibacterial activity compared to

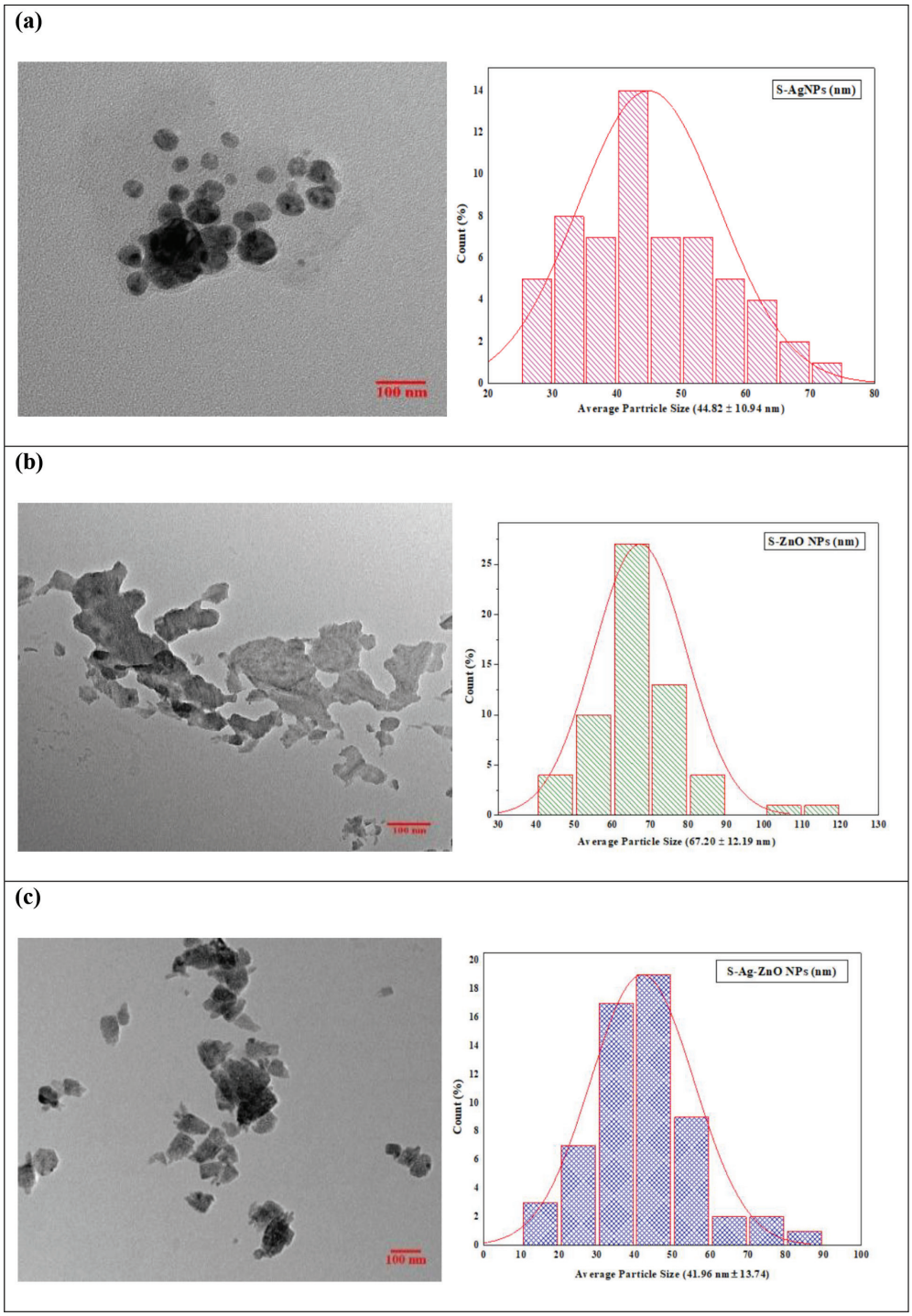

Figure 8. TEM images (including inset histograms showing average particle size) of (a) S-AgNPs, (b) S-ZnO NPs, and (c) S-Ag-ZnO NPs, synthesized using S.E.

the reference antibiotics. The majority of the bacterial strains showed inhibition zones of 21 to 29 mm against ampicillin. Ciprofloxacin showed inhibition zones of 30.0 ± 0.5 mm, 26.50 ± 0.50 mm, and 27.70 ± 0.25 mm against *P. aeruginosa*, *K. pneumoniae*, and *S. marcescens*, respectively. The broad-spectrum antibacterial activity of the synthesized NPs was observed in the disc diffusion assay, and the maximum zones of inhibition were observed for the S-Ag-ZnO NPs (Table 2) under the experimental conditions. The antibacterial activity observed in the present study was comparable to the activity reported for the previously published Ag-ZnO-based nanomaterials synthesized by a green route and tested under similar experimental conditions (Table 2) and (Fig. 9) [43]. Under the current experimental conditions, the synthesized NPs formulations with S-Ag-ZnO NPs showed relatively larger inhibition zones and lower observed MIC and MBC values than the respective monometallic NPs. The enhanced antibacterial activity might be related to the combined presence of Ag and ZnO and physicochemical properties such as particle size, morphology, surface properties, crystallinity, and dispersion. Gram-negative bacteria were more susceptible than Gram-positive bacteria, which may be associated with the differences in cell envelope

structure. The relatively thin peptidoglycan layer and outer membrane of Gram-negative bacteria have been reported to facilitate interactions with NPs, while the thicker peptidoglycan layer of Gram-positive bacteria may reduce NPs penetration [44]. Similarly, the study of Samoilova *et al.* [45] demonstrated that, in comparison to Gram-positive bacteria, Ag/ZnO nanostructures had a relatively higher antibacterial activity against Gram-negative bacteria and speculated that this could be related to improved interactions between the nanomaterials and the bacterial surface. Silver-based NPs have also been reported to disrupt the integrity of bacterial membranes and hence increase the susceptibility of bacteria to antibacterial agents [46]. Several studies have suggested that the antibacterial activity of Ag- and ZnO-based nanomaterials may be attributed to multiple mechanisms such as ROS generation, release of Ag^{+} and Zn^{2+} ions, membrane disruption, and inhibition of essential cellular functions like respiration, membrane potential, DNA replication, and protein synthesis [47]. Furthermore, it has been reported that the antibacterial performance is influenced by the characteristics of NPs such as particle size, morphology, surface charge, crystal structure, and colloidal dispersion. The relatively smaller particle size and better dispersion of S-Ag-ZnO NPs in the present study may increase the effective surface area for interaction with bacterial cells, which may contribute to the observed antibacterial activity. Almutairi [48] reported similar findings and suggested that the enhanced antibacterial activity of Ag-ZnO nanohybrids could be attributed to the release of Ag^{+} and Zn^{2+} ions, increased ROS generation, and disruption of bacterial membrane integrity. Although several antibacterial mechanisms of Ag-ZnO-based nanomaterials were previously proposed, these mechanisms were not directly investigated in the present work. Thus, the enhanced antibacterial activity of the S-Ag-ZnO NPs should be interpreted as an experimental finding under the synthesis conditions used, but not as definitive evidence of a specific combined or mechanistic interaction between Ag and ZnO. Further mechanistic studies, such as ROS quantification, ion-release analysis, and membrane integrity assays, are required to elucidate the precise antibacterial mechanisms responsible for the observed activity [49]. Although S-Ag-ZnO NPs exhibited superior biological activities compared with the corresponding monometallic NPs, the synthesis conditions were optimized individually according to their distinct formation mechanisms and were therefore not compositionally matched. In addition, quantitative determination of the Ag:Zn elemental composition and compositionally matched AgNP + ZnO physical

Table 1. The MIC/MBC analysis of monometallic (S-AgNPs and S-ZnO NPs) and bimetallic (S-Ag-ZnO NPs).

Tested Bacterial Strain	µg/ml	S-AgNPs	S-ZnO NPs	S-Ag-ZnO NPs	Ampicillin/ Ciprofloxacin	S.E.
Gram (+)	MIC	7.81	15.625	3.9	2	ND
Enterococcus faecium	MBC	31.25	31.25	15.625	8	ND
Enterococcus faecalis	MIC	15.625	31.25	7.81	2	ND
	MBC	62.5	125	31.25	8	ND
Staphylococcus aureus	MIC	15.625	62.5	7.81	0.25	62.5
	MBC	62.5	250	31.25	1	250
Bacillus subtilis	MIC	31.25	62.5	15.625	0.5	31.25
	MBC	125	250	62.5	2	125
Gram (-) *Escherichia coli*	MIC	3.9	7.81	1.95	0.5	ND
	MBC	15.625	62.5	7.81	2	ND
Pseudomonas aeruginosa	MIC	15.625	62.5	7.81	0.5	ND
	MBC	62.5	250	31.25	1	ND
Serratia marcescens	MIC	31.25	62.5	15.625	0.031	ND
	MBC	125	250	62.5	0.125	ND
Klebsiella pneumoniae	MIC	31.25	62.5	15.625	0.125	ND
	MBC	125	250	31.25	0.5	ND

Table 2. The inhibitory effects of S- AgNPs, S-ZnO NPs, and S-Ag-ZnO NPs were assessed by determining the diameter of inhibition zones against different bacterial strains.

Tested Bacterial Gram (+) or (-) strains	Concentration (200 µg/ml)				
	S-AgNPs	S-ZnO NPs	S-Ag-ZnO NPs	S.E.	Ampicillin (10 µg/disc) / Ciprofloxacin (5 µg/disc) (+) control
Enterococcus faecium	9.25 ± 0.25[a]	6.85 ± 0.35[a]	11.1 ± 0.4[a]	ND	22.5 ± 0.70
Enterococcus faecalis	9.7 ± 0.1[a]	7.8 ± 0.6[a]	10.5 ± 0.1[a]	ND	26.25 ± 0.35
Staphylococcus aureus	7.9 ± 0.1[a]	5.85 ± 0.15[a]	9.8 ± 0.2[a]	5.5 ± 0.7[a]	29 ± 1.41
Bacillus subtilis	10.3 ± 0.3[a]	7.4 ± 0.4[a]	11.35 ± 0.15[a]	ND	25.5 ± 0.70
Escherichia coli	9.7 ± 0.1[a]	7.5 ± 0.5[a]	10.75 ± 0.25[a]	ND	24.5 ± 0.70
Pseudomonas aeruginosa	10.9 ± 0.1[a]	7.5 ± 0.5[a]	12.4 ± 0.4[a]	ND	30 ± 0.5
Serratia marcescens	11.15 ± 0.15[a]	8.25 ± 0.25[a]	12.25 ± 0.25[a]	ND	27.7 ± 0.25
Klebsiella pneumoniae	10.65 ± 0.15[a]	7.8 ± 0.2[a]	11.5 ± 0.15[a]	ND	26.50 ± 0.5

ND means not detected. [a] Indicates a statistically significant difference ($p < 0.05$) relative to the control.

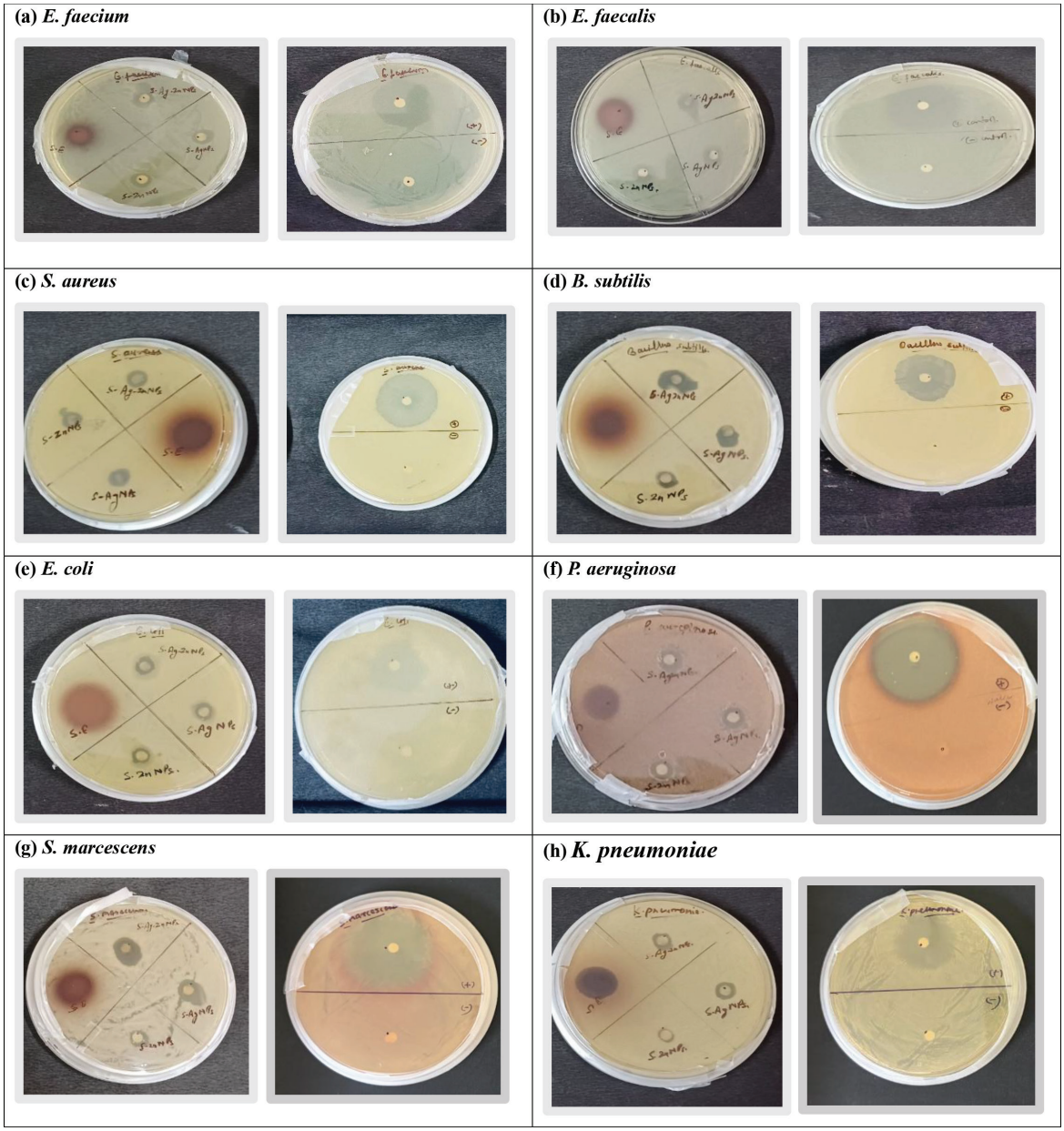

Figure 9. The disc diffusion technique was used to evaluate the antibacterial activities of S.E., S-AgNPs, S-ZnO NPs, and S-Ag-ZnO NPs against both Gram-positive and Gram-negative bacterial strains. The positive control was ampicillin and ciprofloxacin, whereas the negative control was sterile ddH_2O.

mixture or metal-equivalent controls were not included in the present study. Consequently, the enhanced biological performance should be interpreted as an experimental observation rather than definitive evidence of a nanohybrid-specific combined effect. Future studies incorporating quantitative elemental analysis and matched control formulations will provide a more rigorous evaluation of the contributions of composition and nanohybrid architecture.

3.8 Antioxidant assays

3.8.1 DPPH, ABTS, superoxide scavenging, and p-NDA assays

The antioxidant potentials of the synthesized NPs and S.E. were evaluated by four complementary assays: DPPH, ABTS, superoxide scavenging, and p-NDA scavenging assays [(Fig. 10) and (Table 3)]. The antioxidant activity of compounds is characterized by their ability to donate an electron or a hydrogen atom to the stable DPPH radical and therefore reduce the DPPH radical absorbance [50]. Similarly, the ABTS assay relies on the reduction of the ABTS radical cation ($ABTS^+$) generated by oxidation of ABTS with potassium persulfate, in which the antioxidant-mediated reduction of $ABTS^+$ results in a reduction in absorbance at 734 nm [51]. The superoxide scavenging assay is based on the measurement of the superoxide anion scavenging activity by monitoring the inhibition of the reduction of NBT by the superoxide radicals generated by the riboflavin-light system [22]. In DPPH, ABTS, and superoxide scavenging assays, all synthesized NPs and S.E. showed radical-scavenging activity in a concentration-dependent manner in the tested concentration range of 2–12 µg/ml. However, none of the synthesized samples showed inhibition >50%

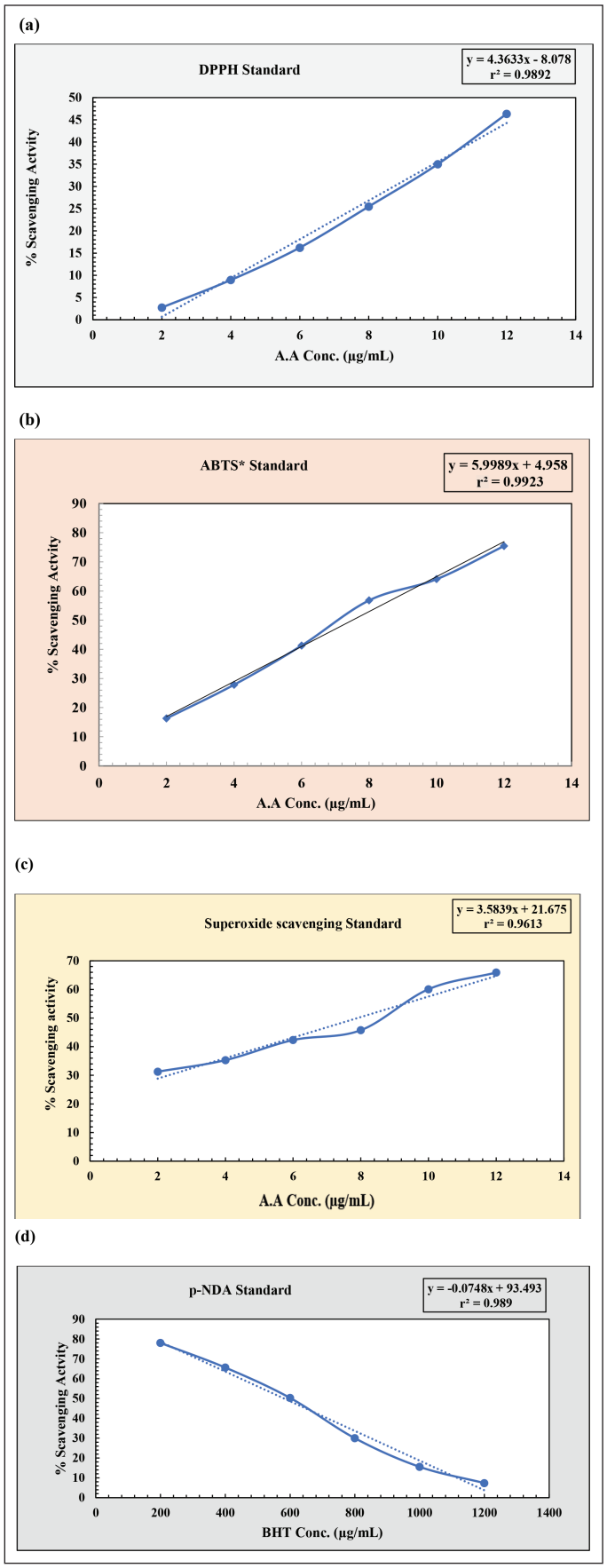

Figure 10. Standard graph of (a) DPPH, (b) ABTS, (c) superoxide scavenging, and (d) p-NDA antioxidant assay.

Table 3. Comparative IC_{50} values (µg/ml) of the synthesized (S-Ag-ZnO NPs S-AgNPs, and S-ZnO NPs), S.E., and standards (A.A/ BHT) in antioxidant assays.

Sample	DPPH IC_{50} (µg/ml)	DPPH Inhibition at 12 µg/ml (%)	ABTS IC_{50} (µg/ml)	ABTS Inhibition at 12 µg/ml (%)	Superoxide scavenging IC_{50} (µg/ml)	Superoxide Inhibition at 12 µg/ml (%)	Hydroxyl Radical IC_{50} (µg/ml)
S-Ag-ZnO NPs	>12	38.60 ± 0.25	>12	36.98 ± 0.67	>12	49.42 ± 0.08	614.62 ± 24.55
S-AgNPs	>12	32.59 ± 0.42	>12	29.41 ± 0.84	>12	42.26 ± 0.21	854.9 ± 10.68
S-ZnO NPs	>12	26.49 ± 0.20	>12	25.35 ± 0.62	>12	33.62 ± 0.26	987.32 ± 22.87
S.E.	>12	23.46 ± 0.98	>12	18.80 ± 0.33	>12	29.53 ± 1.05	1078 ± 11.39
A.A	>12	46.35 ± 0.84	7.5	76.25 ± 1.35	7.9	65.89 ± 1.12	–
BHT	–	–	–	–	–	–	581.50 ± 11

— Indicates that the sample was not evaluated in the corresponding assay.

at this concentration, and thus their IC_{50} values are reported as >12 µg/ml. Thus, the antioxidant activities of the synthesized NPs in these assays were compared on the basis of the experimentally determined percentage inhibition at the highest tested concentration (12 µg/ml).

Among the synthesized nanomaterials, S-Ag-ZnO NPs exhibited the maximum radical-scavenging activity with inhibition values of 38.60% ± 0.25%, 36.98% ± 0.67%, and 49.42% ± 0.08% in DPPH, ABTS, and superoxide scavenging assays, respectively, followed by S-AgNPs, S-ZnO NPs, and S.E. These results revealed that S-Ag-ZnO NPs showed relatively higher antioxidant activity at the concentration range tested. Sarkar *et al.* [52] reported similar observations, showing significant ABTS radical-scavenging activity of green-synthesized Ag/ZnO nanodots using *Artemisia austroyunnanensis* leaf extract. The nanodots showed considerable radical-scavenging activity in the ABTS assay with an IC_{50} value of 31.85 µg/ml. The relatively higher antioxidant activity of S-Ag-ZnO NPs compared with S-AgNPs and S-ZnO NPs under the present experimental conditions may be associated with the combined presence of Ag, ZnO, and leaf-extract phytochemicals. However, the specific mechanisms involved in this activity were not studied.

Under suitable chemical conditions, hydrogen peroxide can take part in the generation of hydroxyl radicals. Hydroxyl radicals are reactive oxygen species that can participate in lipid peroxidation and cellular injury. In the p-NDA assay, the iron-EDTA complex reacts with hydrogen peroxide to generate hydroxyl radicals, which react with and bleach p-NDA. The extent of p-NDA bleaching is reduced in the presence of antioxidants or radical scavengers. Therefore, the inhibition of p-NDA bleaching in the presence of the synthesized NPs suggests their ability to scavenge hydroxyl radicals under the experimental conditions [53]. P-NDA assay results were obtained as IC_{50} values for all samples, in contrast to the DPPH, ABTS, and superoxide scavenging assays. BHT was used as a positive control and had the lowest IC_{50} value (581.50 ± 11.00 µg/ml). Among the synthesized NPs, S-Ag-ZnO NPs showed the highest hydroxyl radical-scavenging activity IC_{50} (614.62 ± 24.55 µg/ml), followed by S-AgNPs (854.90 ± 10.68 µg/ml), S-ZnO NPs (987.32 ± 22.87 µg/ml), and the S.E. (1078.22 ± 11.39 µg/ml). The antioxidant activity of synthesized NPs was generally in the order of S.E. < S-ZnO NPs < S-AgNPs < S-Ag-ZnO NPs. This comparison for the DPPH, ABTS, and superoxide scavenging assays is made at the highest tested concentration (12 µg/ml) based on the percentage of inhibition, whereas for the hydroxyl radical scavenging assay it is based on the experimentally determined IC_{50} values. The higher antioxidant activity of S-Ag-ZnO NPs may be attributed to the combined effect of Ag, ZnO, and phytochemical surface capping agents. However, the exact mechanisms, including the scavenging of reactive oxygen species and electron-transfer processes, were not explored in the present study. Similar observations were reported previously [54]. Aththanayaka *et al.* [55] also reported enhanced antioxidant activity of phytogenic $Ag/Ag_2O/ZnO$ nanocomposites in comparison with monometallic nanocomposites because of the presence of metal oxide components and phytochemical capping agents. Plant phytochemicals present in the plant extract and bound to the surface of green-synthesized ZnO NPs might also be responsible for their antioxidant activity and free-radical-scavenging capacity, as observed for plant-mediated ZnO NPs [56]. The higher antioxidant activity of S-Ag-ZnO NPs in the present study may thus be due to the presence of Ag, ZnO, and phytochemical surface coating. However, the present study did not explore the specific interactions between these components.

4. CONCLUSION

The purpose of this work was to effectively show the immediate microwave-assisted green synthesis of silver nanoparticles, S-ZnO NPs, and S-Ag-ZnO NPs using the leaf extract of *S. cumini* (L.) as a reducing and stabilizing agent. Nanoparticle production was encouraged by the high phenolic and flavonoid contents of the extract, which were validated by UV-vis, DLS, zeta potential, FTIR, X-ray diffraction, TEM, and SEM investigations. The synthesized nanoparticles exhibited hydrodynamic sizes of 125, 87, and 92 nm, average TEM particle sizes of 44.82 ± 10.94, 67.20 ± 12.19, and 41.96 ± 13.74 nm, and zeta potential values of –35, –23, and –14 mV for S-AgNPs, S-ZnO NPs, and S-Ag-ZnO NPs, respectively. Among the synthesized nanomaterials, S-Ag-ZnO NPs exhibited the smallest particle size together with the strongest antibacterial activity, showing the largest inhibition zones and the lowest MIC/MBC values against the tested bacterial strains. In addition, S-Ag-ZnO NPs exhibited comparatively higher radical-scavenging activity than the corresponding monometallic nanoparticles in the DPPH, ABTS, and superoxide scavenging assays at the highest tested concentration (12 µg/ml), while also demonstrating the lowest experimentally determined IC_{50} value among the synthesized nanoparticles in the p-NDA assay. Overall, these results suggest that S-Ag-ZnO NPs have the potential to be used as green nanomaterials for antimicrobial and antioxidant applications. Future studies should investigate the long-term colloidal stability, Ag^+ ion release, biocompatibility, and *in vivo* efficacy of the synthesized nanoparticles to further establish their biomedical and environmental applicability. In addition, quantitative Ag:Zn elemental analysis together with compositionally matched AgNP + ZnO physical mixture and metal-equivalent controls should be included to better distinguish the effects of composition from those arising from the nanohybrid structure.

5. ACKNOWLEDGMENT

The authors are thankful to SAIF, AIIMS (New Delhi) for providing facilities for TEM studies.

6. AUTHOR CONTRIBUTIONS

All authors made substantial contributions to conception and design, acquisition of data, or analysis and interpretation of data; took part in drafting the article or revising it critically for important intellectual content; agreed to submit to the current journal; gave final approval of the version to be published; and agree to be accountable for all aspects of the work. All the authors are eligible to be authors as per the International Committee of Medical Journal Editors (ICMJE) requirements/guidelines.

7. FUNDING

There is no funding to report.

8. CONFLICTS OF INTEREST

The authors report no financial or any other conflicts of interest in this work.

9. ETHICAL APPROVALS

This study does not involve experiments on animals or human subjects.

10. DATA AVAILABILITY

All the data are available with the authors and shall be provided upon request.

11. PUBLISHER'S NOTE

All claims expressed in this article are solely those of the authors and do not necessarily represent those of the publisher, the editors, and the

reviewers. This journal remains neutral with regard to jurisdictional claims in published institutional affiliation.

12. USE OF ARTIFICIAL INTELLIGENCE (AI)-ASSISTED TECHNOLOGY

The authors declare that they have not used artificial intelligence (AI)-tools for writing and editing of the manuscript, and no images were manipulated using AI.

REFERENCES

1. Jha S, Rani R, Singh S. Biogenic zinc oxide nanoparticles and their biomedical applications: a review. J Inorg Organomet Polym Mater 2023;33(6):1437–52; doi: https://doi.org/10.1007/s10904-023-02550-x
2. Kumar A, P N, Kumar M, Jose A, Tomer V, Oz E, *et al.* Major phytochemicals: recent advances in health benefits and extraction method. Molecules 2023;28:887; doi: https://doi.org/10.3390/molecules28020887
3. Sharifi-Rad M, Elshafie HS, Pohl P. Green synthesis of silver nanoparticles (AgNPs) by Lallemantia royleana leaf extract: their bio-pharmaceutical and catalytic properties. J Photochem Photobiol A Chem 2024;448:115318; doi: https://doi.org/10.1016/j.jphotochem.2023.115318
4. Sharifi-Rad M, Pohl P. Synthesis of biogenic silver nanoparticles (AgCl-NPs) using Pulicaria vulgaris Gaertn. aerial part extract and their application as antibacterial, antifungal and antioxidant agents. Nanomaterials 2020;10:638; doi: https://doi.org/10.3390/nano10040638
5. El-Gebaly AS, Sofy AR, Hmed AA, Youssef AM. Green synthesis, characterization and medicinal uses of silver nanoparticles (Ag-NPs), copper nanoparticles (Cu-NPs) and zinc oxide nanoparticles (ZnO-NPs) and their mechanism of action: a review. Biocatal Agric Biotechnol 2024;55:103006; doi: https://doi.org/10.1016/j.bcab.2023.103006
6. Zhang S, Chen J, Ma Y, Zhao Q, Jing B, Yu M, *et al.* Green synthesis, biomedical effects, and future trends of Ag/ZnO bimetallic nanoparticles: an update. Nanotechnol Rev 2025;14(1):20250186; doi: https://doi.org/10.1515/ntrev-2025-0186
7. Qamar M, Akhtar S, Ismail T, Wahid M, Abbas MW, Mubarak MS, *et al.* Phytochemical profile, biological properties, and food applications of the medicinal plant *Syzygium cumini*. Foods 2022;11:378; doi: https://doi.org/10.3390/foods11030378
8. Srivastava S, Chandra D. Pharmacological potentials of *Syzygium cumini*: a review. J Sci Food Agric 2013;93(9):2084–93; doi: https://doi.org/10.1002/jsfa.6111
9. Chagas VT, França LM, Malik S, Paes AMA. *Syzygium cumini* (L.) Skeels: a prominent source of bioactive molecules against cardiometabolic diseases. Front Pharmacol 2015;6:259; doi: https://doi.org/10.3389/fphar.2015.00259
10. Priya SH, Prakasan N, Purushothaman J. Antioxidant activity, phenolic-flavonoid content and high-performance liquid chromatography profiling of three different variants of *Syzygium cumini* seeds: a comparative study. J Intercult Ethnopharmacol 2017;6(1):107–14; doi: https://doi.org/10.5455/jice.20161229055555
11. Kumar A, Tyagi PK, Tyagi S, Ghorbanpour M. Integrating green nanotechnology with sustainable development goals: a pathway to sustainable innovation. Discov Sustain 2024;5:364; doi: https://doi.org/10.1007/s43621-024-00610-x
12. Mellinas C, Jiménez A, Garrigós MDC. Microwave-assisted green synthesis and antioxidant activity of selenium nanoparticles using Theobroma cacao L. bean shell extract. Molecules 2019;24(22):4048; doi: https://doi.org/10.3390/molecules24224048
13. Singleton VL, Orthofer R, Lamuela-Raventós RM. Analysis of total phenols and other oxidation substrates and antioxidants by means of Folin–Ciocalteu reagent. Methods Enzymol 1999;299:152–78; doi: https://doi.org/10.1016/S0076-6879(99)99017-1
14. Quettier-Deleu C, Gressier B, Vasseur J, Dine T, Brunet C, Luyckx M, *et al.* Phenolic compounds and antioxidant activities of buckwheat (Fagopyrum esculentum Moench) hulls and flour. J Ethnopharmacol 2000;72(1–2):35–42; doi: https://doi.org/10.1016/S0378-8741(00)00196-3
15. Pauzi N, Mat Zain N, Ahmad Yusof NA. Microwave-assisted synthesis of ZnO nanoparticles stabilized with gum arabic: effect of microwave irradiation time on ZnO nanoparticles size and morphology. Bull Chem React Eng Catal 2019;14(1):182–8; doi: https://doi.org/10.9767/bcrec.14.1.3320.182-188
16. Kumar PN, Vijayakumar B, Ranjith R. Microwave assisted green synthesis of ZnO nanotubes using Amorphophallus paeoniifolius tuber extract. IOP Conf Ser Mater Sci Eng 2021;1070:012136; doi: https://doi.org/10.1088/1757-899X/1070/1/012136
17. Chung E, Ren G, Johnston I, Matharu RK, Ciric L, Walecka A, *et al.* Applied methods to assess the antimicrobial activity of metallic-based nanoparticles. Bioengineering 2023;10:1259; doi: https://doi.org/10.3390/bioengineering10111259
18. Ahmed S, Saifullah, Ahmad M, Swami BL, Ikram S. Green synthesis of silver nanoparticles using Azadirachta indica aqueous leaf extract. J Radiat Res Appl Sci 2016;9(1):1–7; doi: https://doi.org/10.1016/j.jrras.2015.06.006
19. More PR, Zannella C, Folliero V, Foglia F, Troisi R, Vergara A, *et al.* Antimicrobial applications of green synthesized bimetallic nanoparticles from Ocimum basilicum. Pharmaceutics 2022;14:2457; doi: https://doi.org/10.3390/pharmaceutics14112457
20. Lee KG, Shibamoto T. Antioxidant property of aroma extracts isolated from clove buds (*Syzygium aromaticum* (L.) Merr. et Perry). Food Chem 2001;74:443–8; doi: https://doi.org/10.1016/S0308-8146(01)00161-3
21. Khuda F, Jamil M, Ali Khan Khalil A, Ullah R, Ullah N, Naureen F, *et al.* Assessment of antioxidant and cytotoxic potential of silver nanoparticles synthesized from root extract of Reynoutria japonica Houtt. Arab J Chem 2022;15:104327; doi: https://doi.org/10.1016/j.arabjc.2022.104327
22. Cheng CW, Chen LY, Chou CW, Liang JY. Investigations of riboflavin photolysis via coloured light in the nitro blue tetrazolium assay for superoxide dismutase activity. J Photochem Photobiol B 2015;148:262–7; doi: https://doi.org/10.1016/j.jphotobiol.2015.04.028
23. Selvan DA, Mahendiran D, Kumar RS, Rahiman AK. Garlic, green tea and turmeric extracts-mediated green synthesis of silver nanoparticles: phytochemical, antioxidant and *in vitro* cytotoxicity studies. J Photochem Photobiol B 2018;180:243–52; doi: https://doi.org/10.1016/j.jphotobiol.2018.02.014
24. Dharmastuti W, Elya B, Hanafi M, Lotulung PDN. Phytochemical constituents, anti-diabetic and antioxidant activities of methanol extracts of Diospyros malabarica (Desr.) Kostel leaves and stem bark. Trop J Nat Prod Res 2024;8(5):7249–58; doi: https://doi.org/10.26538/tjnpr/v8i5.29
25. Sukmasari S, Mohd FN, Qader OAJA, Rahman MNA. Total phenolic content, flavonoid content, and antioxidant capacity of *Syzygium cumini* (L.) Skeels leaves grown in Wonosobo, Java, Indonesia and comparison against current findings of *Syzygium cumini* leaves and Syzygium polyanthum (Wight) Walp leaves. J Pharm Sci Res 2018;10(1):31–5.
26. Ghosh S, Goudar VS, Padmalekha KG, Bhat SV, Indi SS, Vasan HN. ZnO/Ag nanohybrid: synthesis, characterization, synergistic antibacterial activity and its mechanism. RSC Adv 2012;2(3):930–40; doi: https://doi.org/10.1039/C1RA00610H
27. Cacua K, Ordoñez F, Zapata C, Herrera B, Pabón E, Buitrago-Sierra R. Surfactant concentration and pH effects on the zeta potential values of alumina nanofluids to inspect stability. Colloids Surf A Physicochem Eng Asp 2019;583:123960; doi: https://doi.org/10.1016/j.colsurfa.2019.123960
28. Parameshwaran R, Kalaiselvam S, Jayavel R. Green synthesis of silver nanoparticles using Beta vulgaris: role of process conditions on size

distribution and surface structure. Mater Chem Phys 2013;140:135–47; doi: https://doi.org/10.1016/j.matchemphys.2013.03.012
29. Souza TG, Ciminelli VS, Mohallem NDS. A comparison of TEM and DLS methods to characterize size distribution of ceramic nanoparticles. J Phys Conf Ser. 2016;733:012039; doi: https://doi.org/10.1088/1742-6596/733/1/012039
30. Vera J, Herrera W, Hermosilla E, Díaz M, Parada J, Seabra AB, *et al.* Antioxidant activity as an indicator of the efficiency of plant extract-mediated synthesis of zinc oxide nanoparticles. Antioxidants (Basel) 2023;12(4):784; doi: https://doi.org/10.3390/antiox12040784
31. Mekky AE, Nashaat MN, Mohamed S, Shehata SM, Abd-Elhamed W, Nada RS, *et al.* Bio-fabrication of silver nanoparticles (AgNPs) using antioxidant-rich *Syzygium cumini* L. leaves extract with the evaluation of its antibacterial and anti-inflammatory activity. Al-Azhar J Agric Res 2023;48(3):460–74; doi: https://doi.org/10.21608/ajar.2023.320590
32. Mendhulkar VD, Kharat SN, Mahadik SR. Plant extract mediated AgNPs synthesis in Averrhoa bilimbi and *Syzygium cumini* leaf extract, their characterization and antioxidant potential assessment. Der Pharma Chem 2018;10(11):24–33.
33. Sivamaruthi BS, Ramkumar VS, Archunan G, Chaiyasut C, Suganthy N, Kesika P, *et al.* Biogenic synthesis of silver–palladium bimetallic nanoparticles from fruit extract of Terminalia chebula: $_{in\ vitro}$ evaluation of anticancer and antimicrobial activity. J Drug Deliv Sci Technol 2019;51:139–51; doi: https://doi.org/10.1016/j.jddst.2019.02.018
34. Hashemi S, Asrar Z, Pourseyedi S, Nadernejad N. Green synthesis of ZnO nanoparticles by Olea europaea. IET Nanobiotechnol 2016;10(6):400–4; doi: https://doi.org/10.1049/iet-nbt.2015.0048
35. Pradhan L, Mounika B, Mukherjee S. Plant leaf-based compounds and their role in nanomaterials synthesis and applications. In: Ghosh S, Ghosh A (eds.). Secondary Metabolites Based Green Synthesis of Nanomaterials and Their Applications, Springer Nature Singapore, Singapore, p 209, 2023; doi: https://doi.org/10.1007/978-981-99-7185-9_10
36. Alharbi NS, Alsubhi NS, Felimban AI. Green synthesis of silver nanoparticles using medicinal plants: characterization and application. J Radiat Res Appl Sci 2022;15(3):109–24; doi: https://doi.org/10.1016/j.jrras.2022.06.012
37. Hashem AH, El-Sayyad GS. Antimicrobial and anticancer activities of biosynthesized bimetallic silver–zinc oxide nanoparticles (Ag–ZnO NPs) using pomegranate peel extract. Biomass Convers Biorefin 2024;14:20345–57; doi: https://doi.org/10.1007/s13399-023-04126-8
38. Rizwana H, Bokahri NA, Alkhattaf FS, Albasher G, Aldehaish HA. Antifungal, antibacterial, and cytotoxic activities of silver nanoparticles synthesized from aqueous extracts of mace-arils of Myristica fragrans. Molecules. 2021;26(24):7709; doi: https://doi.org/10.3390/molecules26247709
39. Devi PG, Velu AS. Synthesis, structural and optical properties of pure ZnO and Co-doped ZnO nanoparticles prepared by the co-precipitation method. J Theor Appl Phys 2016;10(3):233–40; doi: https://doi.org/10.1007/s40094-016-0221-0
40. Bankole OM, Omosebi JG. In-situ reduction synthesis and antibacterial evaluation of Cu/Ni complexes derived from hexadecylamine dithiocarbamate. Sci Res Ann Phys Sci 2025;1(2):28–35; doi: https://doi.org/10.63112/0dvg8j42
41. Divya MJ, Sowmia C, Joona K, Dhanya KP. Synthesis of zinc oxide nanoparticle from Hibiscus rosa-sinensis leaf extract and investigation of its antimicrobial activity. Res J Pharm Biol Chem Sci 2013;4(2):1137–42.
42. Chen X, Zhu L, Ma Z, Wang M, Zhao R, Zou Y, *et al.* Ag nanoparticles decorated ZnO nanorods as multifunctional SERS substrates for ultrasensitive detection and catalytic degradation of Rhodamine B. Nanomaterials 2022;12(14):2394; doi: https://doi.org/10.3390/nano12142394
43. Mtavangu SG, Machunda RL, van der Bruggen B, Njau KN. In situ facile green synthesis of Ag–ZnO nanocomposites using Tetradenia riparia leaf extract and its antimicrobial efficacy on water disinfection. Sci Rep 2022;12:15359; doi: https://doi.org/10.1038/s41598-022-19403-1
44. Ranjithkumar B, Kumar ER, Srinivas M, Ramalingam HB, Srinivas C, Magesh G, *et al.* Evaluation of structural, surface morphological and thermal properties of Ag-doped ZnO nanoparticles for antimicrobial activities. Phys E 2021;133:114801; doi: https://doi.org/10.1016/j.physe.2021.114801
45. Samoilova NA, Krayukhina MA, Naumkin AV, Korlyukov AA, Anuchina NM, Popov DA. Polymer-stabilized silver (gold)–zinc oxide nanoheterodimer structures as antimicrobials. Appl Sci 2023;13(20):11121; doi: https://doi.org/10.3390/app132011121
46. Vasiliev G, Kubo AL, Vija H, Kahru A, Bondar D, Karpichev Y, *et al.* Synergistic antibacterial effect of copper and silver nanoparticles and their mechanism of action. Sci Rep 2023;13(1):9202; doi: https://doi.org/10.1038/s41598-023-36460-2
47. Arora N, Thangavelu K, Karanikolos GN. Bimetallic nanoparticles for antimicrobial applications. Front Chem 2020;8:412; doi: https://doi.org/10.3389/fchem.2020.00412
48. Habes Almutairi H. Greenly engineered bimetallic Ag–ZnO nanohybrids for synergistic antibacterial enhancement. J Saudi Chem Soc 2024;28(4):101899; doi: https://doi.org/10.1016/j.jscs.2024.101899
49. Basavegowda N, Baek KH. Multimetallic nanoparticles as alternative antimicrobial agents: challenges and perspectives. Molecules 2021;26(4):912; doi: https://doi.org/10.3390/molecules26040912
50. Suresh P, Doss A, Praveen Pole RP, Devika M. Green synthesis, characterization and antioxidant activity of bimetallic (Ag–ZnO) nanoparticles using Capparis zeylanica leaf extract. Biomass Convers Biorefinery 2024;14(14):16451–9; doi: https://doi.org/10.1007/s13399-023-03743-7
51. Prior RL, Wu X, Schaich K. Standardized methods for the determination of antioxidant capacity and phenolics in foods and dietary supplements. J Agric Food Chem 2005;53(10):4290–302; doi: https://doi.org/10.1021/jf0502698
52. Sarkar K, Dey S, Farhat Z, Kumar A, Choudhuri C, Chowdhury M. Ag/ZnO nanodots from Artemisia austroyunnanensis as antibacterial and anticancer agents against human neuroblastoma cells. Sci Rep 2025;15(1):22598; doi: https://doi.org/10.1038/s41598-025-07251-8
53. Rehana D, Mahendiran D, Kumar RS, Rahiman AK. $_{In\ vitro}$ antioxidant and antidiabetic activities of zinc oxide nanoparticles synthesized using different plant extracts. Bioprocess Biosyst Eng 2017;40(6):943–57; doi: https://doi.org/10.1007/s00449-017-1758-2
54. Mohamed MYA, Ferjani H, Ogunjinmi OE, Jalouli M, Onwudiwe DC, Otitoju TA, *et al.* Phyto-mediated synthesis of Ag, ZnO, and Ag/ZnO nanoparticles from leaf extract of Solanum macrocarpon: evaluation of their antioxidant and anticancer activities. Inorg Chim Acta 2024;569:122086; doi: https://doi.org/10.1016/j.ica.2024.122086
55. Aththanayaka S, Thiripuranathar G, Ekanayake S. Microwave-assisted phytogenic Ag/Ag_2O/ZnO nanocomposite as a replacement of Ag/Ag_2O and ZnO nanoparticles: a comparative antioxidant study. Surf Inter 2023;43:103547; doi: https://doi.org/10.1016/j.surfin.2023.103547
56. Sivasankarapillai VS, Krishnamoorthy N, Eldesoky GE, Wabaidur SM, Islam MA, Dhanusuraman R, *et al.* One-pot green synthesis of ZnO nanoparticles using Scoparia dulcis plant extract for antimicrobial and antioxidant activities. Appl Nanosci 2023;13(9):6093–103; doi: https://doi.org/10.1007/s13204-022-02610-7

How to cite this article:
Jha S, Yadav P, Gahlawat D, Singh S. Green synthesis of silver, zinc oxide, and Ag–ZnO nanoparticles using *Syzygium cumini* leaf extract: Microwave-assisted synthesis, characterization, and biological activities. J Appl Biol Biotech 2027;15(1):181-195. DOI: 10.7324/jabb.2026.319867